AD-A192 482 SIGNIFICANCE OF THE LOCAL ELECTRODE POTENTIAL WITHIN PITS CREVICES AND CRACKS(U) PENNSYLVANIA STATE UNIV UNIVERSITY PARK DEPT OF MATERIALS SCI H W PICKERING 1/1

UNCLASSIFIED FEB 88 N00014-84-K-0201 F/G 7/4 NL

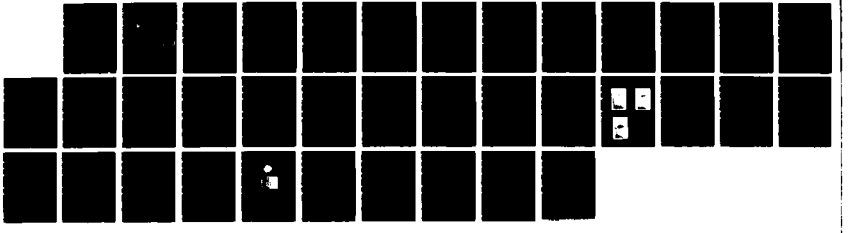

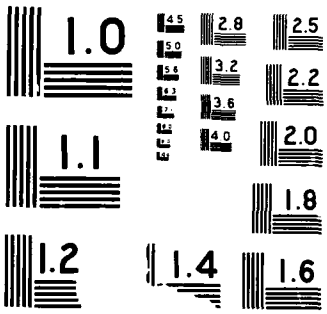
1.0
1.1
1.2
1.4
1.6
1.8
2.0
2.2
2.5
2.8
3.2
3.6
4.0
4.5
5.0

College of Earth and Mineral Sciences

PENNSTATE

DEPARTMENT OF MATERIALS SCIENCE

METALLURGY PROGRAM

TECHNICAL REPORT

February 1988

OFFICE OF NAVAL RESEARCH

Contract No. N00014-84-k-0201

SIGNIFICANCE OF THE LOCAL ELECTRODE POTENTIAL WITHIN PITS, CREVICES AND CRACKS

Howard W. Pickering

Department of Materials Science and Engineering
The Pennsylvania State University

SECURITY CLASSIFICATION OF THIS PAGE *(When Data Entered)*

REPORT DOCUMENTATION PAGE		READ INSTRUCTIONS BEFORE COMPLETING FORM
1. REPORT NUMBER NOOO14-84-k-0201	2. GOVT ACCESSION NO.	3. RECIPIENT'S CATALOG NUMBER
4. TITLE *(and Subtitle)* SIGNIFICANCE OF THE LOCAL ELECTRODE POTENTIAL WITHIN PITS, CREVICES AND CRACKS		5. TYPE OF REPORT & PERIOD COVERED Technical Report 6. PERFORMING ORG. REPORT NUMBER
7. AUTHOR*(s)* H. W. Pickering		8. CONTRACT OR GRANT NUMBER*(s)* NOOO14-84-k-0201
9. PERFORMING ORGANIZATION NAME AND ADDRESS Penn State University University Park, PA 16802		10. PROGRAM ELEMENT, PROJECT, TASK AREA & WORK UNIT NUMBERS
11. CONTROLLING OFFICE NAME AND ADDRESS		12. REPORT DATE February 1988 13. NUMBER OF PAGES
14. MONITORING AGENCY NAME & ADDRESS*(if different from Controlling Office)*		15. SECURITY CLASS. *(of this report)* 15a. DECLASSIFICATION/DOWNGRADING SCHEDULE

16. DISTRIBUTION STATEMENT *(of this Report)*

17. DISTRIBUTION STATEMENT *(of the abstract entered in Block 20, if different from Report)*

18. SUPPLEMENTARY NOTES

19. KEY WORDS *(Continue on reverse side if necessary and identify by block number)*

20. ABSTRACT *(Continue on reverse side if necessary and identify by block number)*

This paper begins with a review of the experimental measurements of the electrode potential within pits, crevices and cracks for several commercially important alloy systems. Then, recent results for crevicing are reviewed. They give further insight into the relationship of the important parameters within the cavity: IR drop, Flade or passivation potential and solution composition, namely that stable crevice corrosion occurs when the electrode potential in the crevice is less oxidizing than

DD FORM 1 JAN 73 1473 EDITION OF 1 NOV 65 IS OBSOLETE
S/N 0102-014-6601

SECURITY CLASSIFICATION OF THIS PAGE *(When Data Entered)*

20. con'd.

the Flade potential of the crevice solution. This result fully supports and contributes to a more detailed understanding of the potential shift mechanism, as originally outlined for pitting in iron, and more recently applied widely to pitting, crevicing, stress corrosion and corrosion fatigue in different alloy systems. Some expected consequences of the potential shift mechanism regarding the initition of localized corrosion are also presented.

SIGNIFICANCE OF THE LOCAL ELECTRODE POTENTIAL WITHIN PITS, CREVICES AND CRACKS

H. W. Pickering
Department of Materials Science and Engineering
The Pennsylvania State University
University Park, PA 16802

ABSTRACT

This paper begins with a review of the experimental measurements of the electrode potential within pits, crevices and cracks for several commercially important alloy systems. Then, recent results for crevicing are reviewed. They give further insight into the relationship of the important parameters within the cavity: IR drop, Flade or passivation potential and solution composition, namely that stable crevice corrosion occurs when the electrode potential in the crevice is less oxidizing than the Flade potential of the crevice solution. This result supports and contributes to a more detailed understanding of the potential shift mechanism , as originally outlined for pitting in iron, and more recently applied widely to pitting, crevicing, stress corrosion and corrosion fatique in different alloy systems. Some expected consequences of the potential shift mechanism regarding the initition of localized corrosion are also presented.

INTRODUCTION

A new school of thought has emerged on localized corrosion and anodic cracking (stress corrosion and corrosion fatigue) that places a great importance on the value of the electrode potential in the cavity[1-6]. In particular, its value with respect to the passivation or Flade potential of the cavity electrolyte may be decisive. With this basis this mechanism provides an understanding of potential as a stabilizing force for pitting and crevice corrosion, and is now being seriously considered in view of supportive results from several laboratories[1-21] on localized corrosion, corrosion fatigue and stress corrosion in iron, steel, aluminum alloys, stainless steels and titanium alloys.

The role of the cavity electrode potential is easily conveyed with the help of the polarization plot shown in Figure 1. When the cavity electrolyte contains an active/passive transition, i.e., a passivation or Flade potential (curve 2), a stable localized corrosion process occurs when the electrode potential in the cavity is less oxidizing than the passivation, E_{pass}, or Flade potential. Then, metal dissolution in the cavity occurs at high rates in the active region of the polarization curve while the outer surface is at a more noble potential in the passive region and dissolves at the low passive rate.

This is in sharp contrast to the traditional view of localized corrosion in which the cavity electrode potential is given no special significance. Rather, changes in the cavity electrolyte are considered to stabilize the active state which allows metal in the cavity to dissolve at the high rates along the dashed curve (1) in Figure 1 while the outer surface dissolves at the low passive rate. Thus, there are two plausible explanations of localized corrosion. Based on the available data for some metal/electrolyte systems, either the potential-shift explanation or a combination of both explanations is applicable. A combination would appear to be necessary when no active loop exists at any potential for the bulk electrolyte composition, a not unusual situation for highly corrosion resistant alloys. The need to create an active loop for crevicing to occur is indicated in the recent results of Shaw, et.al.[21] for some corrosion-resistant, commercial Ni base alloys.

The results that are supportive of the above described role of potential in localized corrosion and environmental cracking are in three forms: (a) the direct measurement of the electrode potential in the cavity (Figure 2), (b) the observation of an electrochemical reaction in the cavity that occurs in a different potential regime than exists at the outer surface, e.g., the occurrence of the hydrogen evolution reaction (h.e.r.) within the cavity but not at the outer surface, and (c) the observation of faceting of pit and crevice walls since this is indicative of film free (Tafel) dissolution, although conditions that give faceting need to be better understood for establishing the reliability of this method.

The potential measurement technique also enables the measurement of the potential drop (IR) within the electrolyte phase, e.g., between points (1) and (2) in sketches 2-left, 3 and 4 of Figure 2. On the other hand, potential drops across solid films on the cavity surface or through bulky solid corrosion products, such as in sketches 1 and 2-right of Figure 2, can not be measured because the Luggin capillary probe can not penetrate them. Hence, any potential drops existing across films would not be measured and would exist in addition to the measured potential drops in the solution. However, from the measured electrode potential in the cavity, and knowing the value of the limiting electrode potential of the metal/electrolyte system[22,23] the maximum possible potential drop across a film on the surface can be determined as the difference in these two values. Hence, information on the upper boundary of a potential drop across a solid film on the surface can be obtained by this measurement technique. In at least one of the above studies[4,5] the difference in these two potentials was very small or nonexistent, indicating the existence of either a film-free active surface or a well conducting (salt) film-covered surface.

Since in the potential-shift mechanism the cavity electrode potential must be below the passivation or Flade potential of the cavity electrolyte for a stable local cell to exist, the IR drop must be greater than a specific value, IR*, where IR* is the difference between the (corrosion or applied) potential at the outer surface and the passivation or Flade potential as shown in Figure 1. Hence, the condition for stability of a local cell (pit, crevice or crack) is that $IR > IR^*$.

Thus, in general, large IR drops within the cavity promote localized corrosion, so it is important to understand the conditions that yield large IR drops in cavities. These include all factors that increase the resistance of the cavity electrolyte such as gas bubbles, or that increase the metal dissolution rate such as a larger maximum current in the active region of the polarization curve of the cavity electrolyte. Geometry, or more specifically , the aspect ratio also plays a major role; the greater the ratio of the depth of the cavity to a particular distance in the plane normal to the depth (narrowness or size of opening), the greater will be the IR drop within the cavity. This geometrical effect has been illustrated and successfully modeled[2]. Considering these factors and based on the available data, a large IR or more specifically the condition IR > IR* can occur when

a) the current path is long, as in a crevice[4,5]

b) gas is present in the cavity, as in pits in iron[1]

c) the crack depth to size of the opening is large, as for corrosion fatigue, hydrogen cracking and stress corrosion cracking[2]

In the case of corrosion fatigue, Gangloff[24] has shown that small crack growth rates are higher than those of larger cracks and that this coincides with an aspect ratio (crack depth to the size of the opening) of small cracks that is greater than for larger cracks. Since the IR drop also increases with increasing aspect ratio[2,6], it follows that the IR > IR* condition may be more readily met for short cracks than for long cracks and that, therefore, metal dissolution more readily occurs at the crack tip, facilitating the crack propagation process in small cracks. This explanation of the higher growth rates of small cracks during corrosion fatigue is an alternative to that previously offered by Gangloff[24] and others based on the traditional view of localized corrosion.

Although the accumulation of gas within pits in iron has been found to be necessary in order for active pitting to occur[1], this is not the case for active crevicing because the length of the current path within crevices in iron is often sufficient by itself to produce an IR that meets the IR>IR* condition, as is shown below. Pits, on the other hand, present a very short current path at early stages, so that the IR > IR* condition is not met except when constrictions to current flow are present within the pit. Hydrogen gas accumulation within pits was shown to be effective in the pitting of iron[1] but, in principle, any gas that accumulates within the pit would be effective, e.g.,

Engell and coworkers[25,26] have reported that nitrogen gas evolves from pits in iron exposed to nitrate solutions. Thus, if the nitrogen gas also accumulates inside the pits into large bubbles that fill the pit cavity as hydrogen has been found to do[1], or if it forms a dispersion of fine N_2 bubbles suspended in the cavity electrolyte as Valdes has observed for H_2 in the crevice electrolyte[4,5], the nitrogen gas will also effectively increase the IR drop in the cavity.

When the IR > IR* condition is met, in addition to stabilizing a localized corrosion process, there are two other important consequences. One, as mentioned above is that different or additional electrochemical reactions may occur in the cavity, e.g., the h.e.r. has been shown to occur inside pits and crevices in iron[1,4,5,8] and aluminum[15] when it does not occur at the outer surface. The other consequence is that the metal dissolution rate within the cavity is strongly potential dependent, since the potential regime in the cavity is in active loop, rather than passive, region. Thus, it is important to know the potential regime within the cavity in order to (a) anticipate the operating reactions and (b) estimate the approximate rate of the local cell process.

Recently, the most complete set of information on a localized corrosion process has been obtained for crevicing of iron by Valdes[4,5]. These results are described next and are in complete agreement with the above described preeminence of the cavity electrode potential in determining whether or not a stable localized corrosion process occurs.

CREVICING IN IRON

The features of a typical crevicing situation are shown in Figure 3. Note that the site of metal dissolution is restricted to a region of the crevice walls that is a certain distance into the crevice from the crevice opening. To the right of this dissolution region, corrosion is not observed, and on the region's left corrosive attack is superficial or nonexistent.

If this geometry of crevice attack is determined by the above described potential-shift mechanism of localized corrosion, then for a corrosion (or applied) potential in the passive region at the outer surface, the electrode potential shifts to less oxidizing values (more negative) with increasing distance into the crevice, and at the boundary of the corroded region, IR=IR* as shown in Figure 3, i.e., at the active/passive boundary $E=E_{pass}$. At yet greater distances into the crevice,

E becomes even more negative as IR increases, and the metal dissolution rate decreases according to the E-i behavior of the active loop of the polarization curve for the cavity electrolyte. At the far boundary of the corroded zone, E is at the mixed potential for the cavity electrolyte (B in Figure 3), or approaches the metal equilibrium potential if no oxidant is present in the cavity solution. Thus, the mixed or equilibrium potential is the limiting potential that can exist in the crevice for the more oxidizing electrode potentials at the outer surface[22,23].

EXPERIMENTAL

This description of the crevicing process follows from results obtained using the experimental set-up shown in Figure 4. With the electrode potential at the outer surface set in the passive region, Valdes[4,5] simultaneously measured and observed the following for an active crevicing situation:

a) E in the crevice (adjustable Luggin capillary attached to a SCE).

b) current flowing out of the crevice

c) whether or not an active/passive boundary forms on the crevice wall

d) location of the active crevicing region on the iron wall of the crevice

e) gas accumulation within the crevice

f) all of the above also for inactive crevicing

The crevice was 10 mm deep and its opening was 0.5 mm by 5 mm, i.e., it was twice as deep as wide as illustrated in Figure 4. The dotted surface of the crevice is iron, whereas the other surfaces of the crevice are the transparent Plexiglass cover plate used to allow direct observation of the iron crevice wall. The other dotted (top) surface is the outer iron surface (approximately twice as large as shown) where the control Luggin capillary was centered.

Several electrolytes were used that differed mainly in pH. Some were well buffered to minimize acidification within the crevice and all of them were free of chloride and other "aggressive" ions so as to eliminate the occurrence of aggressive ion buildup in the crevice. Hence, the only parameter of the three that can readily change appreciably in the crevice (for the buffered electrolytes) is the electrode potential. Thus, it was possible to determine quite

conclusively any relation that might exist between active (and inactive) crevicing and the crevice electrode potential, without the usual uncertainty regarding contributions due to acidification and/or aggressive ion buildup in the crevice. Four of the electrolytes were:

a) 0.001M H_2SO_4; pH=3.4

b) 0.5M acetic acid/0.5M sodium acetate; pH=4.8

c) 0.3M boric acid/0.075M decahydrated sodium borate ($Na_2B_4O_7 \bullet 10H_2O$); pH=8.5

d) 0.1M NaOH; pH=12

The limiting (mixed) potential deep in the crevice could have been due to both oxygen reduction and hydrogen ion discharge, since the cell was open to the air. After establishing that a cathodic pretreatment (-1.00 V SCE) had no effect on the resulting trends in any of the parameters (electrode potential, current flow out of the crevice, H_2 formation, or the development of an active/passive boundary on the crevice wall), most experiments were begun by switching the outer surface control potential from a cathodic value to an anodic value in the passive region. In addition, in order to minimize the effect of hydrogen gas accumulation in the crevice, the hydrogen gas formed during the cathodic polarization pretreatment was removed by physically displacing it just before switching the potential, or some experiments were conducted by directly immersing the sample at a potential in the passive region. All measurements were made at 25 ± 2°C. The potentials are reported on the saturated calomel electrode (SCE) scale.

RESULTS AND DISCUSSION

Developments on the crevice wall are shown in Figure 5. The double vertical line down the middle is the fine (~0.2 mm outer diameter) Luggin capillary used to measure the electrode potential in the crevice. In this sequence of photographs the end of the Luggin capillary is near the crevice bottom; thus, the electrode potential near the bottom is measured. The circles are hydrogen gas bubbles that are growing due to the occurrence of the h.e.r. in the deeper portion of the crevice where the electrode potential is reducing with respect to the h.e.r.. The outer (top) surface of the iron sample is in the passive region, as is the crevice wall down to the horizontal line indicated by the arrow in the 1-minute photograph. Below this line the electrode potential is below the

passivation or Flade potential and iron dissolution occurs at a high rate characteristic of the active region.

This active/passive boundary moves upwards before stabilizing after over one hour. Thus, the IR drop increases with time (assuming the IR* is relatively independent of time since acidification in the crevice is minimized by the buffering action of the solution). The increase in IR is due to an increasing R caused by an increase in the volume fraction of hydrogen gas in the crevice with time. It is also due to an increasing rate of metal dissolution, as indicated by the increasing current flowing out of the crevice (Figure 6). The electrode potential at the bottom of the crevice is also shown in Figure 6, and is over one volt less oxidizing than (negative of) the outer surface value. It decreases in the first few minutes to near the limiting potential. Unlike the case of the pitting of iron where extensive hydrogen gas accumulation was necessary for the IR > IR* condition to be met[1], large IR drops were routinely encounted in the one-cm deep crevice (without accumulation of gas) because of the long current path and currents in the mA range.

The potential profile after 30 min as a function of distance into the crevice is shown in Figure 7. The bottom two-thirds of the crevice is near the limiting potential of the system, consistent with the relative lack of dissolution in this region (Figure 5). Just below the passivation potential, the rate of metal dissolution is highest, in accord with the maximum in the active region (Figure 3).

The above results, showing active crevicing, were typical for both the pH 3 and pH 5 solutions. In order to determine if a one-to-one correspondence exists between a crevice electrode potential that is less or more oxidizing than the Flade potential and active or inactive crevicing, respectively, the above measurements and observations were also made in an electrolytic solution for which the entire crevice wall passivated when a potential in the passive region was applied to the outer surface. This situation occurred for two different solution compositions, the alkaline (pH 9 and 12) solutions and the inhibited acid (pH 3 and 5) solutions. In both cases of inactive crevicing the measured electrode potential everywhere in the crevice was found to be near to (within a few tens of mV) the outer surface value, indicating that the IR > IR* condition was not met even early in the experiment when the current was highest while the passive film was forming.

This measured crevice potential in the passive region is shown in Figure 8 for the 0.1M sodium chromate (inhibited) pH 5 solution and in Figure 9 for the pH 9 solution. At low concentrations of the inhibitor (0.005 and 0.01M) in Figure 8 active crevicing occurred and the potential was in the active regime just as without the inhibitor. This one-to-one correspondence was consistently found: $E_{crevice}$ was significantly shifted from the potential at the outer surface to a value less oxidizing than the passivation or Flade potential when active crevicing occurred, and $E_{crevice}$ was only slightly different from the outer surface value and well within the passive region when the crevice was inactive.

The likely explanation for the inactivity of the crevice for the alkaline and the well inhibited acid solutions is that IR* is larger because an increasing pH or inhibitor concentration shifts the passivation potential, E_{pass}, in the less oxidizing direction corresponding to a reduction in the size of the active loop. For the pH 9, pH 12 and 0.1M inhibited acid solutions, E_{pass} shifted several hundred mV to more negative values. The IR* value was, therefore, increased by this amount making it much more difficult for the IR > IR* condition to be met. This observed shift in passivation potential and increase in IR* are illustrated in Figure 10 as a function of pH. An additional contributing factor is that the IR drop decreases because the size of the active loop and, therefore, the maximum available current decreases with increasing pH or addition of an inhibitor. Chloride ion may also affect the IR > IR* condition, although no results on chloride ion were obtained in these experiments.

Passive Film Breakdown/Pit Initiation. The sequence of photographs in Figure 5 shows that the upper passivated portion of the crevice wall decreases in size with increase in time. This is due to the upward movement of the active/passive boundary. Its movement mirrors an increasing IR in the cavity caused by the increasing current (Figure 6) and increasing R (increase in fractional volume of gas in the crevice), i.e., the IR* position (active/passive interface) shifts towards the crevice mouth. This shift is also shown by the measured potential profiles, which become steeper with time during the initial transient period. This means that a portion of the passive film dissolves

with increasing time during this initial transient period as more and more of the wall aquires a potential below the Flade potential.

Passive film dissolution under the IR > IR* condition was also shown in another experiment. After the crevice wall was completely passivated in the pH 9 or 12 solution, the cell was simultaneously drained and filled with the pH 3 or 5 solution. Within minutes the electrode potential in the crevice shifted to much less oxidizing potentials below E_{pass}, the current increased sharply and an active/passive interface appeared on the crevice wall as the passive film dissolved below this interface. This simultaneous change in the electrode potential in the crevice and in the current flowing out of the crevice is shown in Figure 9. The explanation for the shift in electrode potential to below the passivation potential, corresponding to IR > IR*, is that both a sharp decrease in IR* occurred for the reason shown in Figure 10 and an increase in IR occurred because of an increase in the passive current at the lower pH.

Two factors that could facilitate passive film breakdown under the IR > IR* condition are (a) attached gas bubbles since they provide microcrevices between the bubble and metal surface as illustrated in Figure 11, and (b) H_2 formation at the metal/passive film interface where more reducing conditions exist (compared to the passive film/aqueous-solution interface) as a result of the potential drop across the passive film as illustrated in Figure 12.

The following result indicates that attached gas bubbles could be a factor in causing local dissolution of the passive film. When the iron surface that contained an attached gas bubble was polarized into the passive region, the passive film formed everywhere except where the bubble was attached to the surface. Instead, corrosive attack occurred in the bubble region as illustrated in Figure 13. Although, it is not physically possible to measure the potential in the microcrevices formed by the bubble and iron wall, it follows from the above results that the IR drop in the microcrevice was significant and caused the electrode potential in the microcrevice to be below the passivation potential of the microcrevice electrolyte.

For an already passivated surface an attached gas bubble provides the same microcrevice, thereby providing for the possibility that the IR > IR* condition will again be met in the

microcrevice. This could lead to dissolution of the passive film and the onset of a stable pitting process. However, because a lower (passive) current is flowing within the microcrevice, the IR > IR* condition is less likely to be met than in the above experiment.

The second factor involving hydrogen formation by reduction of H_2O or H^+ ion at the metal/film interface is intriguing and has not been previously considered. It becomes a possibility because the large voltage drop across the passive film (Figure 12) considerably reduces the oxidizing power (or conversely increases the reducing power) of the system at the metal/passive film interface. Thus, if protons or H_2O within the passive film migrate in the direction of the metal/passive film interface they may be reduced and the products H or H_2 may degrade the integrity of the passive film.

CONCLUSIONS

Based on the recent results of Valdes[4,5] on crevicing in iron in solutions free of aggressive ions and buffered to reduce pH changes, it is now clear that:

1. The cavity electrolyte contains an active/passive transition. This result precludes the possibility of explaining the crevicing action by the traditional ideas involving only acidification and/or aggressive ion build up in the crevice.

2. Instead, this and other results indicated that stable active crevicing occurs when the electrode potential in the crevice is less oxidizing than the passivation (or Flade) potential of the crevice electrolyte, $E_{crevice} < E_{pass}$, corresponding to the condition IR > IR*.

3. Acidification of the electrolyte or addition of an inhibitor modifies the crevicing tendency through their modification of both IR* and the IR drop within the cavity.

4. Gas accumulation inside the crevice is not a requirement for crevicing, as it is for pitting, because of the long electrolyte path for current flow, i.e., the IR > IR* condition can be met without the presence of constrictions in the crevice.

5. Conceptually, this potential shift mechanism can also participate in the passive film breakdown/pit initiation process.

6. These results fully support and contribute to a more detailed understanding of the potential shift mechanism, as originally outlined for pitting in iron[1] and more recently applied widely to pitting, crevicing and cracking in different alloy systems.

ACKNOWLEDGMENT

B. W. Parks helped with the preparation of this manuscript. Financial support by the Office of Naval Research under Contract No. N00014-84K-0201 is also gratefully acknowledged.

REFERENCES

1. H. W. Pickering and R. P. Frankenthal, J. Electrochem. Soc., 119, 1297 and 1304, (1972).

2. B. G. Ateya and H. W. Pickering, J. Electrochem. Soc., 122, 1018, (1975).

3. D. Harris and H. W. Pickering, "On Anodic Cracking During Cathodic Hydrogen Charging":, in Effect of Hydrogen on the Behavior of Materials, A. W. Thompson, I. M. Bernstein and A. J. West, eds., Metallurgical Soc. of AIME, Warrendale, PA p. 229, 1976; D. Harris, M.S. Thesis, The Pennsylvania State University, 1975.

4. A. Valdes, Ph.D. thesis, The Pennsylvania State University, 1987.

5. A. Valdes and H. W. Pickering, "IR Drops and The Local Electrode Potential During Crevicing of Iron", in International Conference on Localized Corrosion, H. S. Isaacs et. al., ed., NACE, Houston, TX, to be published.

6. H. W. Pickering and A. Valdes, "A Review of the Effect of Gas Bubbles and Cavity Dimensions on the Local Electrode Potential Within Pits, Crevices and Cracks", in Embrittlement by the Localized Crack Environment, R. P. Gangloff, ed, Metallurgical Soc. of AIME, Warrendale, PA p. 33, 1984.

7. J. Newman, Localized Corrosion, R. W. Staehle, B. F. Brown, J. Kruger, A. Agrawal, Eds., National Association of Corrosion Engineers, Houston, Texas, p. 45, 1975.

8. G. Herbsleb and H. J. Engell, Z. Elektrochem., 65, 881, (1961).

9. N. Stolica, Corrosion Sci., 9, 205, (1969).

10. G. Karlberg and G. Wranglen, Corrosion Sci., 11, 499, (1971).

11. W. D. France and N. D. Greene, Corrosion, 24, 247, (1968).

12. N. D. Greene, W. D. France, Jr., B. E. Wilde, Corrosion, 21, 275, (1965).

13. C. M. Chen, F. H. Beck, M. G. Fontana, Corrosion, 27, 234, (1971).

14. P. Forchhammer and H. J. Engell, Werkst. Korros., 20, 1, (1969).

15. C. B. Bargeron and R. C. Bensen, J. Electrochem. Soc., 127, 2528, (1980).

16. J. A. Davis, "Use of Microelectrodes for Study of Stress Corrosion of Aluminum Alloys", in Localized Corrosion, R. W. Staehle et al., eds., NACE, Houston, TX, p. 168, 1975.

17. R. A. H. Edwards, "Potential Drop and Concentration changes in Stress Corrosion Cracks in 7075 Alloy in Halide Solutions", in Corrosion and Exploitation of the Corrosion of Aluminum Alloys, Holroyd, Scamens and Fields, Eds., Alcon International, 1984.

18. A. Turnbull and M. K. Gardner, British Corrosion, J., 16, 140, (1981).

19. R. A. H. Edwards and P. Schuitemaker, "Determination of Crack Tip pH and Electrode Potential during Corrosion Fatigue of Steels", in Corrosion Chemistry within Pits, Crevices and Cracks, A. Trunbull, Ed., Her Majesty's Stationery Office, London, p. 453, 1987.

20. K. Landles, J. Congleton, and R. N. Parkins, "Potential Measurements Along Actual and Simulated Cracks", in corrosion Chemistry within Pits, Crevices and Cracks, A. trunbull, Ed., Her Majesty's Stationery Office, London, p. 453, 1987.

21. B. Shaw, P. Moran and P. O. Gartland, Extended Abstracts, Vol. 87-2, Abs. 270, The Electrochem. Soc., Pennington, N.J. (1987); B. Shaw, private communication, 1987.

22. H. W. Pickering, H. H. Uhlig, Symp. Corrosion and Corrosion Protection, R. P. Frankenthal, F. Mansfeld, Eds., Electrochemical Society, Pennington, NJ, p. 85, 1981.

23. H. W. Pickering, Corrosion, 42, 125, (1986).

24. R. P. Gangloff, Metallurgical Trans. A, 16A, 953 (1985).

25. A. Baumel and H. J. Engell, Arch. Eisenhuttenwes, 32, 379 (1961).

26. H. J. Engell, K. Bohnenkamp and A. Baumel, Arch. Eisenhuttenwes, 33, 285 (1962).

FIGURE CAPTIONS

Figure 1. Schematic polarization curves of the electrolyte within the pit, crevice or crack for the traditional mechanisms (curve 1) and the potential shift mechanism (curve 2).

Figure 2. Schematic illustrating the different forms of constriction affecting the IR drop in the cavity. The application of a potential measuring probe for these different situations is discussed in the text.

Figure 3. Schematic illustrating the relation between the local cell site in the crevice and the polarization curve of the crevice solution for a sample polarized to potential A in the passive region. The nonpassivated area deeper into the crevice (below E_{lim}) is at the mixed potential of the cavity solution.

Figure 4. Schematic of the sample arrangement and experimental setup. The two highlighted areas are surfaces in contact with the electrolyte. After Harris[3].

Figure 5. Photographs, through the Plexiglas, of the iron wall of the crevice during anodic polarization of the outer (top) iron surface at +0.6V (SCE) in 0.5 M acetic acid - 0.5 M sodium acetate (solution b). above the line shown by the pointer (1 minute), the crevice passivates. Iron dissolution is rapid in the region shown by the bracket. Mag. 7X. From Valdes[4,5].

Figure 6. Electrode potential near the bottom of the crevice and current flowing out of the crevice as a function of time for the conditions in Figure 5. From Valdes[4,5].

Figure 7. Electrode potential profile into the crevice after 30 minutes for the conditions in Figure 5. From Valdes[4,5].

Figure 8. Electrode Potential Profiles in the crevice for different concentrations of sodium chromate for quasistationary conditions (values at 2 to 3 hrs). The sample was anodically polarized (outer surface) at +1.0 V (SCE) in solution b. From Valdes[4,5].

Figure 9. Electrode potential measured at the bottom of the crevice and measured cell current before and after changing from pH 9 (solution c) to pH 5 (solution b). The sample was anodically polarized in the passive region at +0.6 V (SCE) for the entire time. From Valdes[4,5].

Figure 10. Schematic illustrating the variation of IR* as a function of pH because of the strong pH dependence of the passivation potential.

Figure 11. Schematic illustrating microcrevices (bold arrows) formed by gas bubbles attached to the surface. Potential shifts caused by currents following out of the microcrevices could cause passive film breakdown and pitting at these sites.

Figure 12. Schematic illustrating a typical potential profile across a passive film. As the voltage drop increases in the aqueous and passive film phases, the oxidizing power decreases (reducing power increases) at the metal/passive film interface.

Figure 13. Localized corrosion at the site of a hydrogen gas bubble (formed during the -1.0V (SCE) pretreatment) adhering to the otherwise passivated surface, during anodic polarization at +0.6V (SCE) in the inhibited (0.1M sodium chromate) solution b. Upper, 30x; Lower, 120x. From Valdes[4,5].

H. W. Pickering Discussion to Group C Presentation

In passive film breakdown, we should consider the occurrence of side reactions at different points in the film since the electrode potential is more negative (more reducing) as one approaches the metal/oxide interface due to the voltage drop across the film. Therefore, species diffusing into the film may become unstable and be reduced, e.g., water or H^+ may be reduced and the resulting H atoms or H_2 gas could then participate in the film breakdown process.

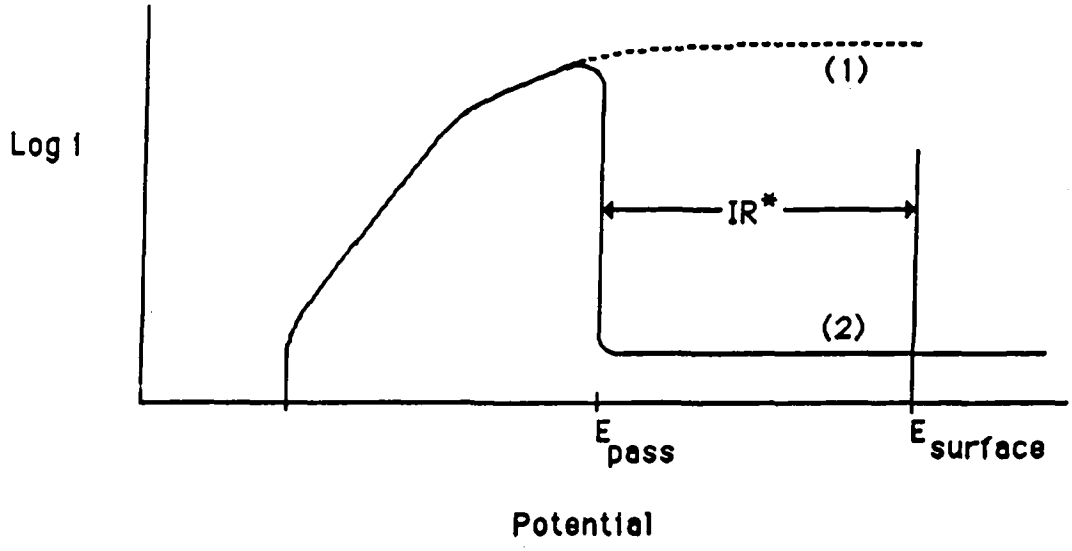
Log I
(1)
IR*
(2)
E pass
E surface
Potential

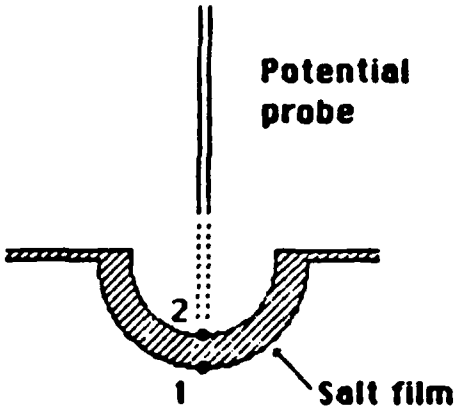

1. Salt film

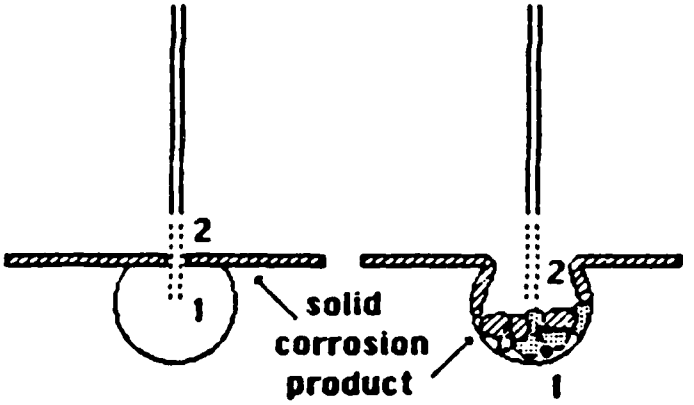

2. Solid Corrosion Product

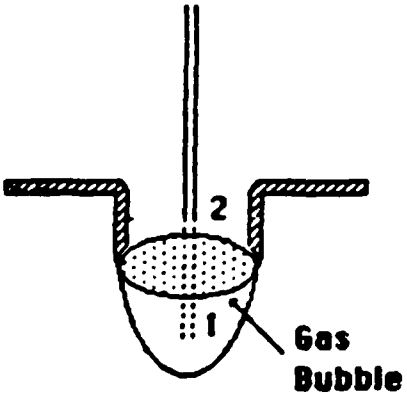

3. Gas accumulation

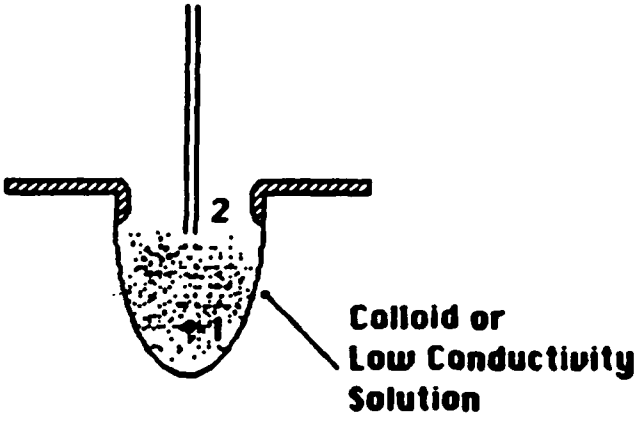

4. Low Conductivity Solution

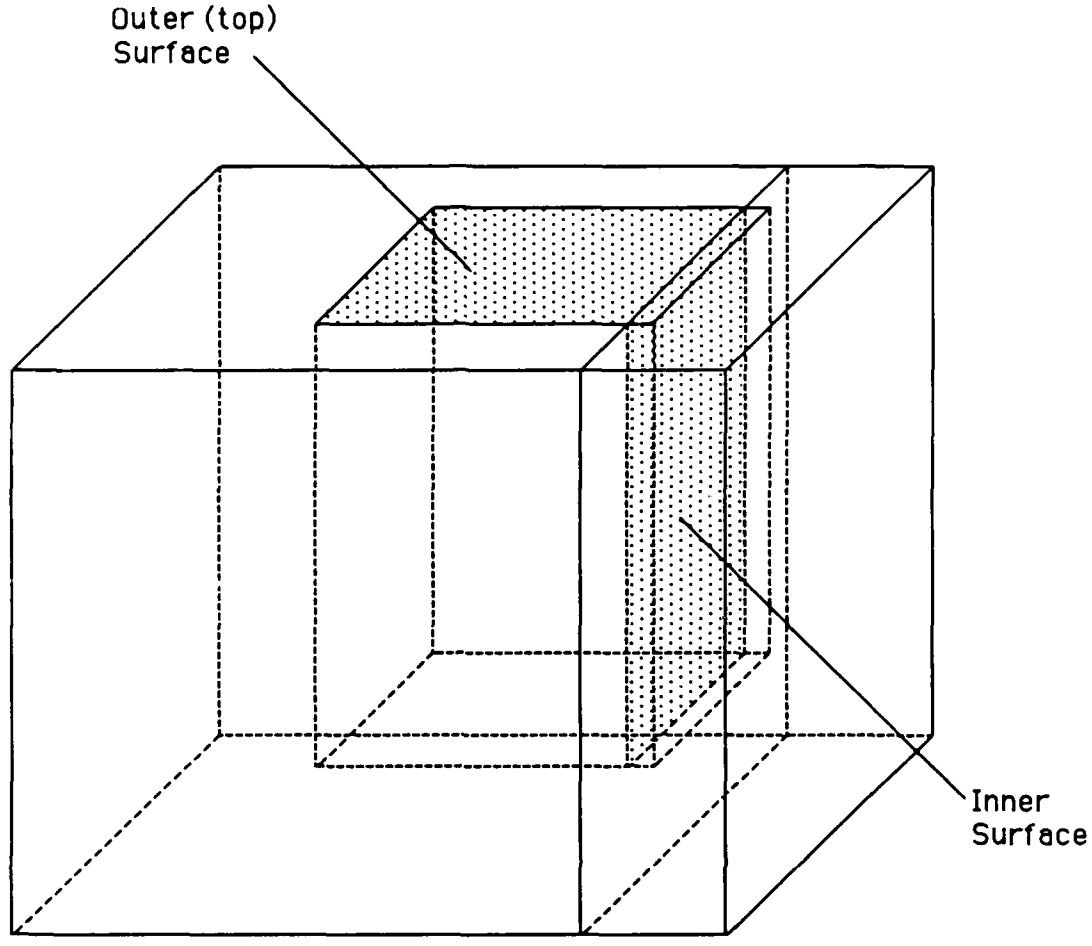
Outer (top)
Surface
Inner
Surface

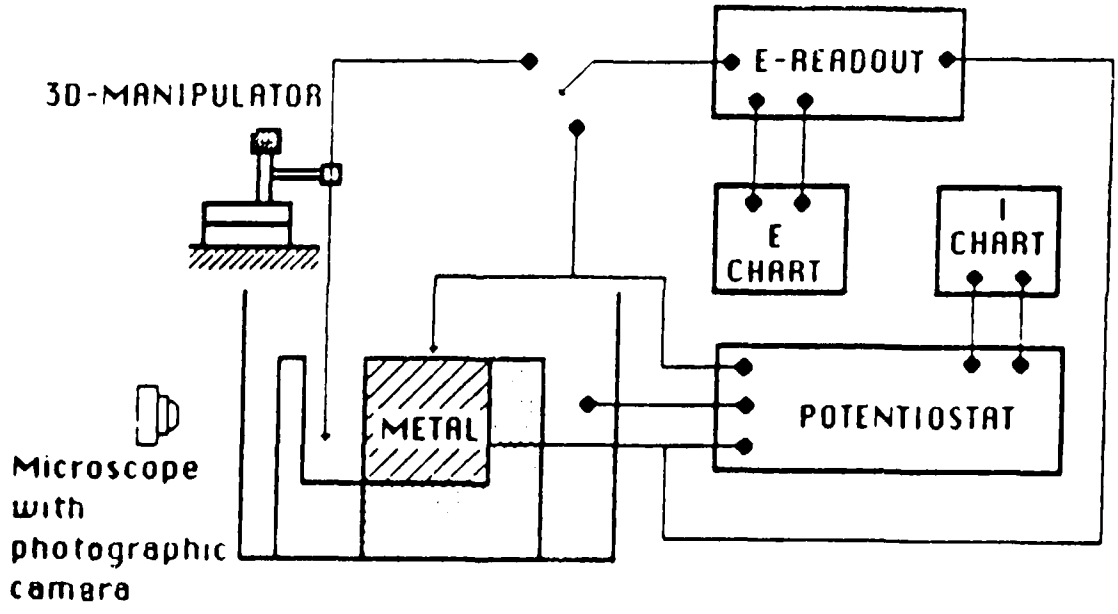
3D-MANIPULATOR
E-READOUT
E
CHART
I
CHART
METAL
POTENTIOSTAT
Microscope
with
photographic
camara

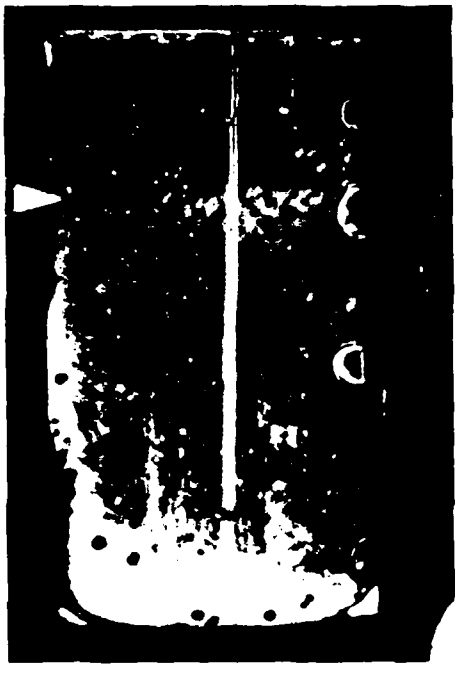

1 minute

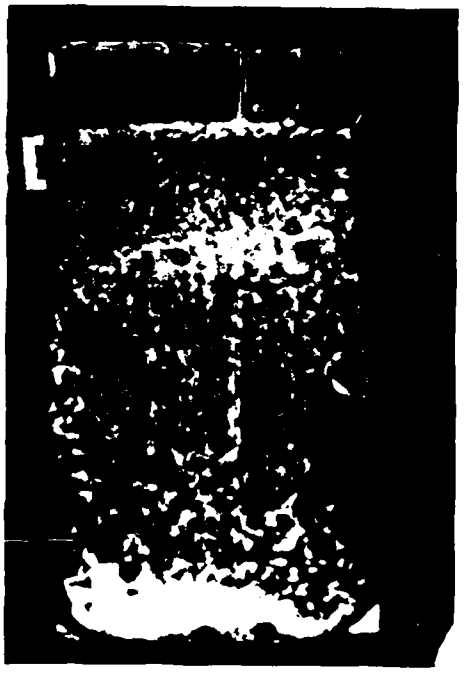

10 minutes

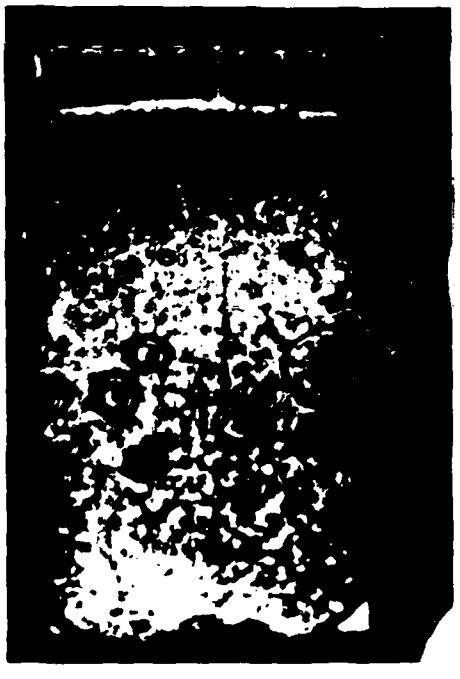

60 minutes

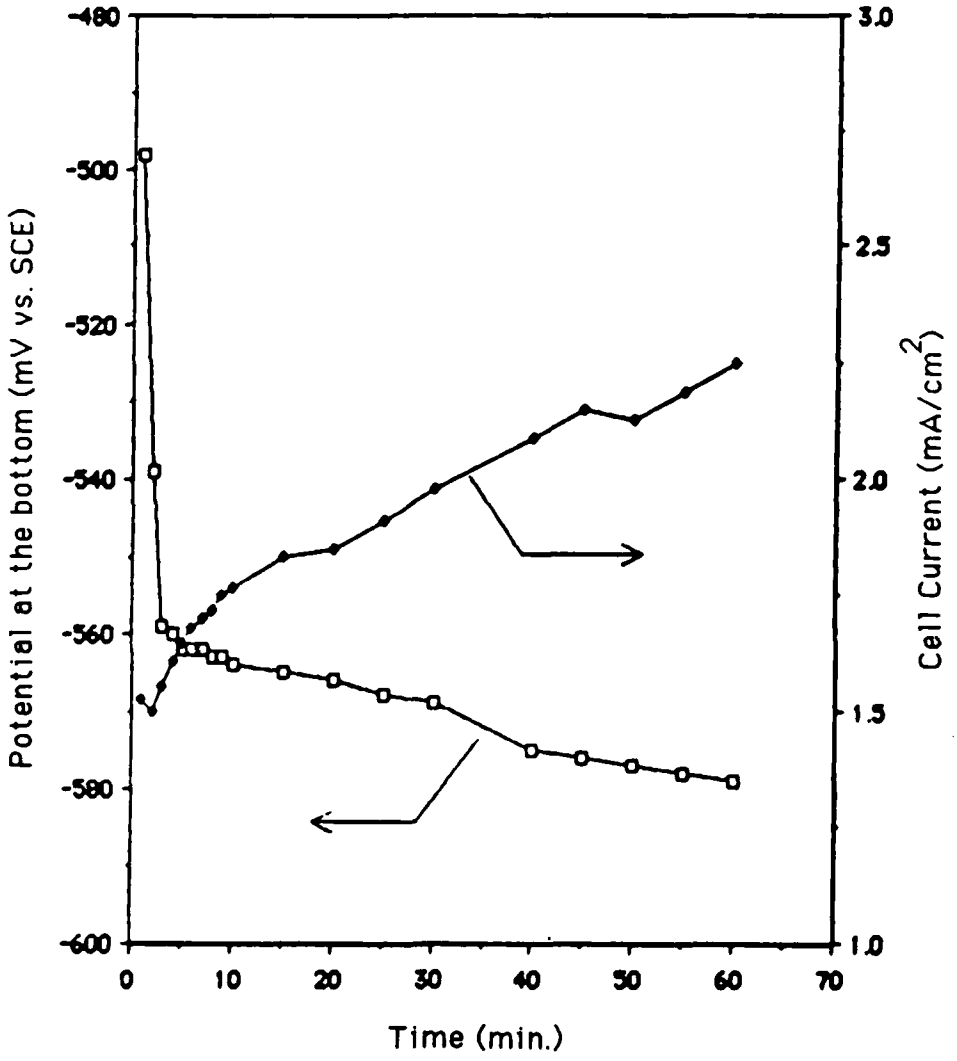

FIG. 6 PICKERING

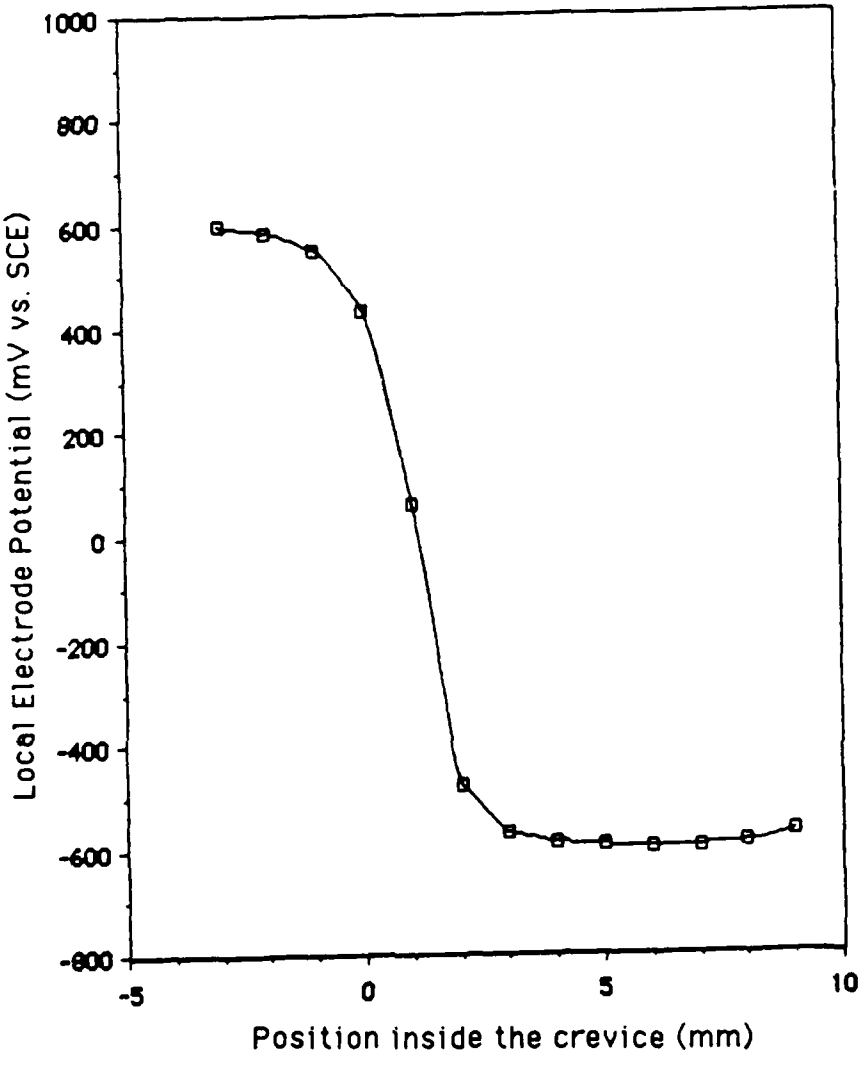
1000
800
600
400
200
0
-200
-400
-600
-800
-5
0
5
10
Local Electrode Potential (mV vs. SCE)
Position inside the crevice (mm)

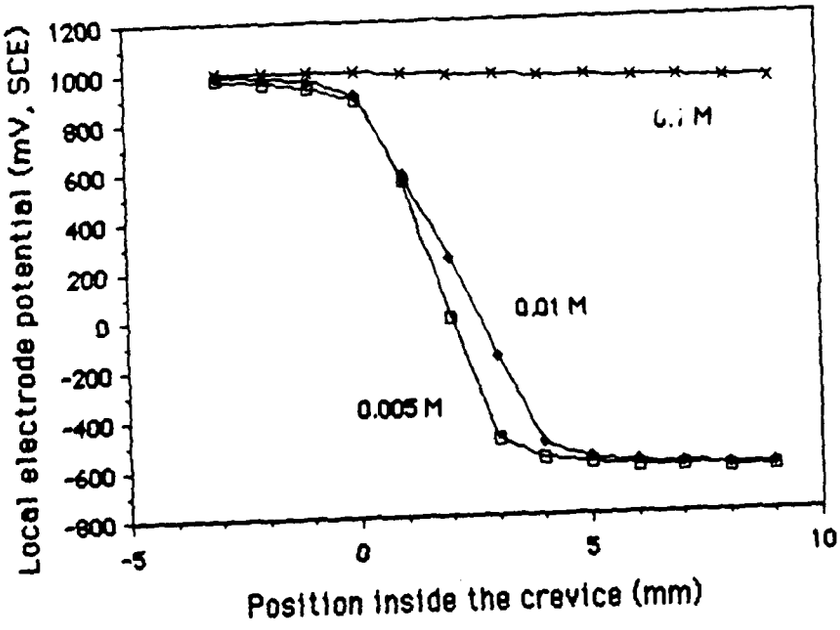
Local electrode potential (mV, SCE)
1200
1000
800
600
400
200
0
-200
-400
-600
-800
-5
0
5
10
Position inside the crevice (mm)
0.1 M
0.01 M
0.005 M

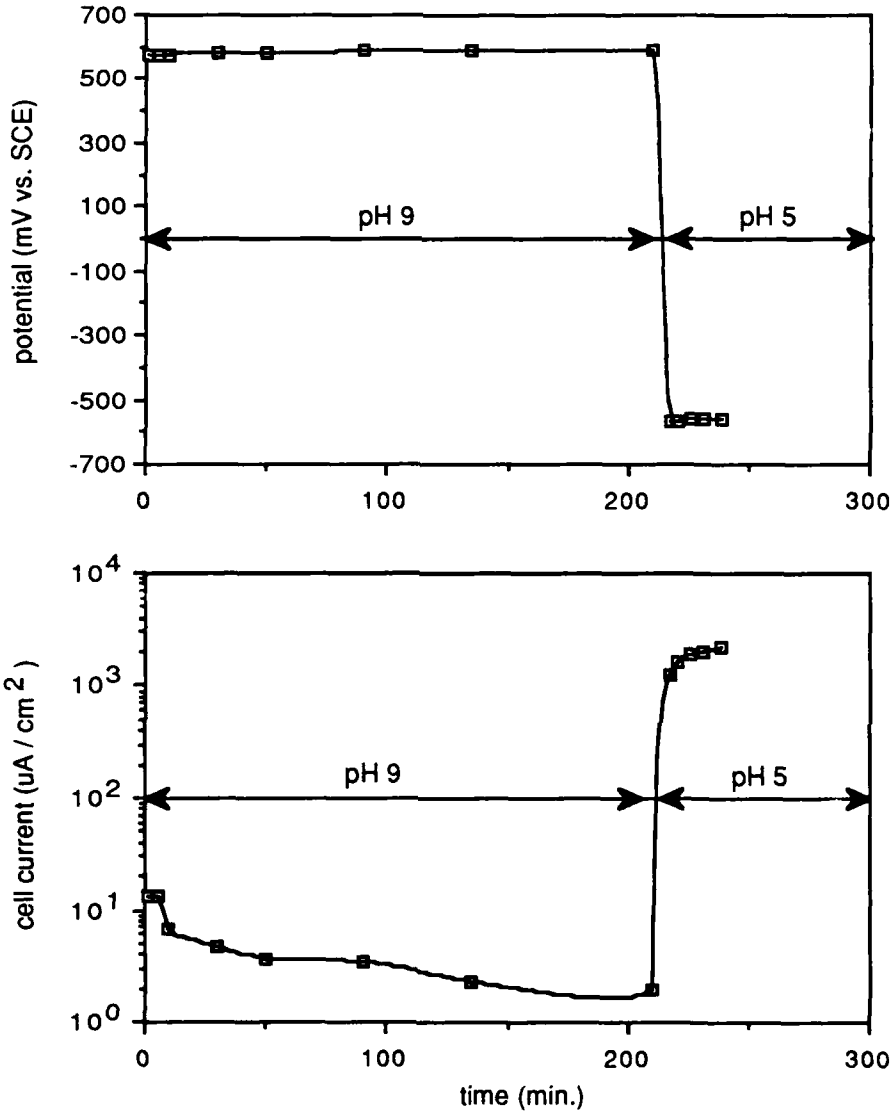
700
500
300
100
-100
-300
-500
-700
potential (mV vs. SCE)
pH 9
pH 5
0
100
200
300
10^4
10^3
10^2
10^1
10^0
cell current (uA / cm^2)
pH 9
pH 5
0
100
200
300
time (min.)

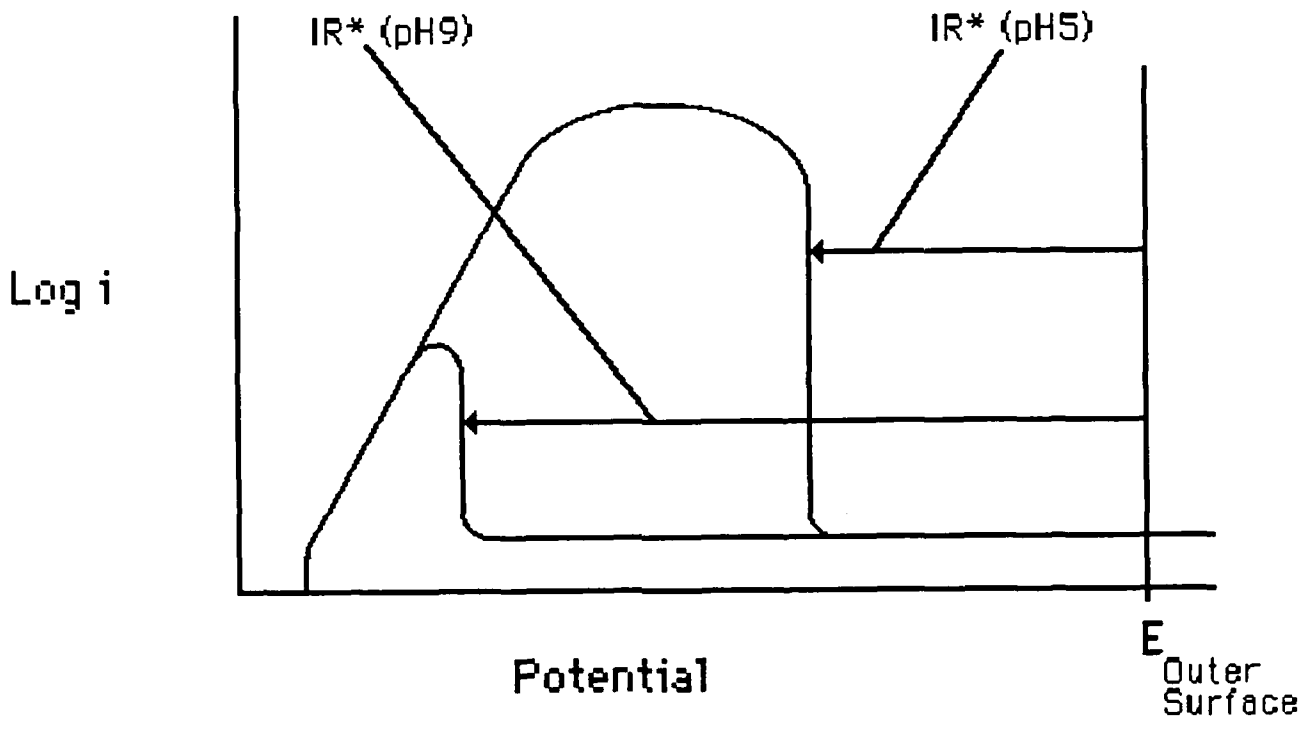
IR* (pH9)
IR* (pH5)
Log i
Potential
E
Outer
Surface

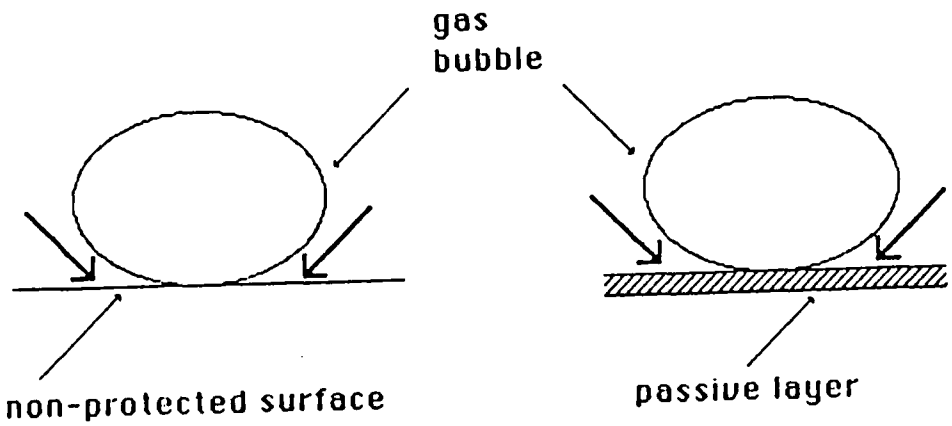

FIG 11 PICKERING

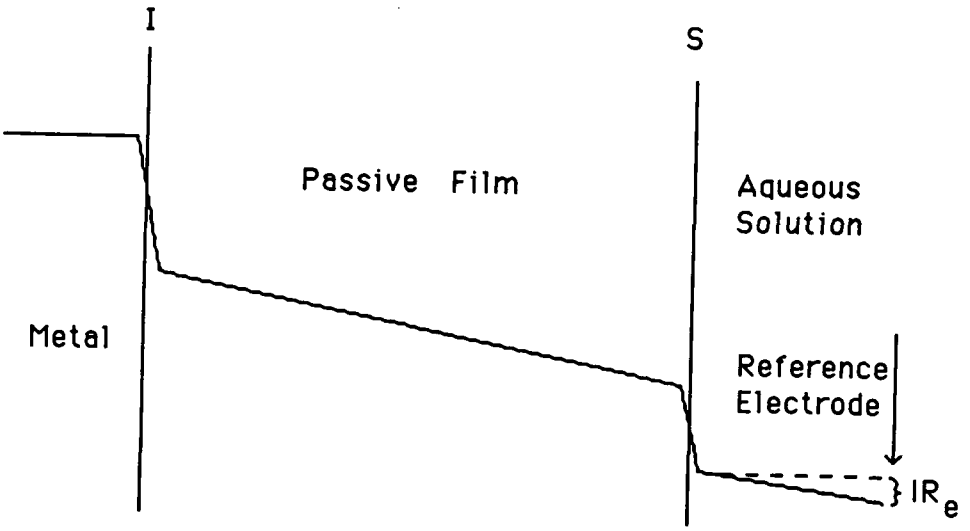

FIG 12 PICKERING

FIG. 13 PICKERING

DEPARTMENT OF THE NAVY
OFFICE OF NAVAL RESEARCH
ARLINGTON, VIRGINIA 22217

IN REPLY REFER TO

BASIC DISTRIBUTION LIST

Technical and Summary Reports 1985

Organization	Copies
Defense Documentation Center Cameron Station Alexandria, VA 22314	12
Office of Naval Research Department of the Navy 800 N. Quincy Street Arlington, VA 22217 Attn: Code 431	3
Naval Research Laboratory Washington, DC 20375 ATTN: Codes 6000 6300 2627	1 1 1
Naval Air Development Center Code 606 Warminster, PA 18974 ATTN: Dr. J. DeLuccia	1
Commanding Officer Naval Surface Weapons Center White Oak Laboratory Silver Spring, MD 20910 ATTN: Library	1
Naval Oceans Systems Center San Diego, CA 92132 ATTN: Library	1
Naval Postgraduate School Monterey, CA 93940 ATTN: Mechanical Engineering Department	1
Naval Air Systems Command Washington, DC 20360 ATTN: Code 310A Code 5304B	1 1
Naval Sea System Command Washington, DC 20362 ATTN: Code 05R	1
Naval Air Propulsion Test Center Trenton, NJ 08628 ATTN: Library	1
Naval Construction Battallion Civil Engineering Laboratory Port Hueneme, CA 93043 ATTN: Materials Division	1
Naval Electronics Laboratory San Diego, CA 92152 ATTN: Electron Materials Sciences Division	1
Naval Missile Center Materials Consultant Code 3312-1 Point Mugu, CA 93041	1
Commander David W. Taylor Naval Ship Research and Development Center Bethesda, MD 20084	1
Naval Underwater System Center Newport, RI 02840 ATTN: Library	1
Naval Weapons Center China Lake, CA 93555 ATTN: Library	1
NASA Lewis Research Center 21000 Brookpark Road Cleveland, OH 44135 ATTN: Library	1
National Bureau of Standards Washington, DC 20234 ATTN: Metals Science and Standards Division Ceramics Glass and Solid State Science Division Fracture and Deformation Div.	1 1 1

Naval Facilities Engineering Command
Alexandria, VA 22331
ATTN: Code 03 1

Scientific Advisor
Commandant of the Marine Corps
Washington, DC 20380
ATTN: Code AX 1

Army Research Office
P. O. Box 12211
Triangle Park, NC 27709
ATTN: Metallurgy & Ceramics Program 1

Army Materials and Mechanics Research Center
Watertown, MA 02172
ATTN: Research Programs Office 1

Air Force Office of Scientific Research/NE
Building 410
Bolling Air Force Base
Washington, DC 20332
ATTN: Electronics & Materials Science Directorate 1

NASA Headquarters
Washington, DC 20546
ATTN: Code RRM 1

General Electric Company
P.O. Box 7722
Philadelphia, PA 19101

Defense Metals and Ceramics Information Center
Battelle Memorial Institute
505 King Avenue
Columbus, OH 43201 1

Metals and Ceramics Division
Oak Ridge National Laboratory
P.O. Box X
Oak Ridge, TN 37380 1

Los Alamos Scientific Laboratory
P.O. Box 1663
Los Alamos, NM 87544
ATTN: Report Librarian 1

Argonne National Laboratory
Metallurgy Division
P.O. Box 229
Lemont, IL 60439 1

Brookhaven National Laboratory
Technical Information Division
Upton, Long Island
New York 11973
ATTN: Research Library 1

Library
Building 50, Room 134
Lawrence Radiation Laboratory
Berkeley, CA 1

Send ONE COPY to each unless otherwise indicated.

Supplemental Distribution List Mar 1987

Prof. I.M. Bernstein
Dept. of Metallurgy and Materials Science
Carnegie-Mellon University
Pittsburgh, PA 15213

Prof. H.K. Birnbaum
Dept. of Metallurgy & Mining Eng.
University of Illinois
Urbana, Ill 61801

Prof. H.W. Pickering
Dept. of Materials Science and Eng.
The Pennsylvania State University
University Park, PA 16802

Prof. D.J. Duquette
Dept. of Metallurgical Eng.
Rensselaer Polytechnic Inst.
Troy, NY 12181

Prof. J.P. Hirth
Dept. of Metallurgical Eng.
The Ohio State University
Columbus, OH 43210

Prof. H. Leidheiser, Jr.
Center for Coatings and Surface Research
Sinclair Laboratory, Bld. No. 7
Lehigh University
Bethlehem, PA 18015

Dr. M. Kendig
Rockwell International - Science Center
1049 Camino Dos Rios
P.O. Box 1085
Thousand Oaks, CA 91360

Prof. R. A. Rapp
Dept. of Metallurgical Eng.
The Ohio State University
Columbus, OH 43210

Profs. G.H. Meier and F.S.Pettit
Dept. of Metallurgical and Materials Eng.
University of Pittsburgh
Pittsburgh, PA 15261

Dr. W. C. Moshier
Martin Marietta Laboratories
1450 South Rolling Rd.
Baltimore, MD 21227-3898

Prof. P.J. Moran
Dept. of Materials Science & Eng.
The Johns Hopkins University
Baltimore, MD 21218

Prof. R.P. Wei
Dept. of Mechanical Engineering and Mechanics
Lehigh University
Bethlehem, PA 18015

Prof. W.H. Hartt
Department of Ocean Engineering
Florida Atlantic University
Boca Raton, Florida 33431

Dr. B.G. Pound
SRI International
333 Ravenswood Ave.
Menlo Park, CA 94025

Prof. C.R. Clayton
Department of Materials Science & Engineering
State University of New York
Stony Brook
Long Island, New York 11794

Prof. Boris D. Cahan
Dept. of Chemistry
Case Western Reserve Univ.
Cleveland, Ohio 44106

Dr. K. Sadananda
Code 6390
Naval Research Laboratory
Washington, D.C. 20375

Prof. M.E. Orazem
Dept. of Chemical Engineering
University of Virginia
Charlottesville, VA 22901

Mr. T.W. Crooker
Code 6310
Naval Research Laboratory
Washington, D.C. 20375

Prof. G.R. St. Pierre
Dept. of Metallurgical Eng.
The Ohio State University
Columbus, OH 43210

Prof. G. Simkovich
Dept. of Materials Science & Eng.
The Pennsylvania State University
University Park, PA 16802

Dr. E. McCafferty
Code 6310
Naval Research Laboratory
Washington, D. C. 20375

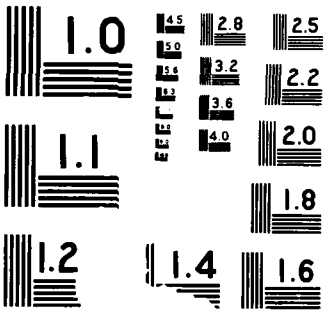
1.0
1.1
1.2
1.4
1.6
1.8
2.0
2.2
2.5
2.8
3.2
3.6
4.0
4.5
5.0